

# Study on the preparation of Mg–Li–Mn alloys by electrochemical codeposition from LiCl–KCl–MgCl<sub>2</sub>–MnCl<sub>2</sub> molten salt

Ke Ye · Mi Lin Zhang · Ye Chen · Wei Han ·

Yong De Yan · Shu Quan Wei · Li Jun Chen

Received: 17 October 2009 / Accepted: 14 February 2010 / Published online: 4 March 2010  
© Springer Science+Business Media B.V. 2010

**Abstract** This study presents a novel electrochemical study on the codeposition of Mg, Li, and Mn on a molybdenum electrode in LiCl–KCl–MgCl<sub>2</sub>–MnCl<sub>2</sub> melts at 893 K to form different phases Mg–Li–Mn alloys. Transient electrochemical techniques such as cyclic voltammetry, chronopotentiometry, and chronoamperometry have been used in order to investigate the codeposition behavior of Mg, Li, and Mn ions. The results obtained show that the potential of Li metal deposition, after the addition of MgCl<sub>2</sub> and MnCl<sub>2</sub>, is more positive than the one of Li metal deposition before the addition. The codeposition of Mg, Li, and Mn occurs at current densities lower than  $-1.43 \text{ A cm}^{-2}$  in LiCl–KCl–MgCl<sub>2</sub> (8 wt%) melts containing 2 wt% MnCl<sub>2</sub>. The onset potential for the codeposition of Mg, Li, and Mn is  $-2.100 \text{ V}$ .  $\alpha$ ,  $\alpha + \beta$ , and  $\beta$  phases Mg–Li–Mn alloys with different lithium and manganese contents were obtained via galvanostatic electrolysis from LiCl–KCl melts with different concentrations of MgCl<sub>2</sub> and MnCl<sub>2</sub>. The microstructures of typical  $\alpha$  and  $\beta$  phases of Mg–Li–Mn alloys were characterized by X-ray diffraction (XRD), optical microscopy (OM), and scanning electron microscopy (SEM). The analysis of energy dispersive spectrometry (EDS) and EPMA area analysis showed that the elements of Mg and Mn distribute homogeneously in the Mg–Li–Mn alloys. The results of inductively coupled plasma analysis determined that the chemical compositions of Mg–Li–Mn alloys correspond

with the phase structures of XRD patterns, and lithium and manganese contents of Mg–Li–Mn alloys depend on the concentrations of MgCl<sub>2</sub> and MnCl<sub>2</sub>.

**Keywords** Mg–Li–Mn alloys · LiCl–KCl–MgCl<sub>2</sub>–MnCl<sub>2</sub> · Molten salt · Electrochemical codeposition · Cyclic voltammetry

## 1 Introduction

The magnesium–lithium alloys are the ultralight constructional metallic materials having density of 1.35–1.65 g cm<sup>-3</sup>, which is 1.5–2.0 times less than that of aluminum alloys and is similar to that of constructional plastics. In addition, Mg–Li alloys also show high specific stiffness, and high electrical and thermal conductivities. These alloys have attracted great attention due to their merits, especially in the fields of aerospace, aircraft, and weapon [1–3]. Despite that, poor corrosion resistance and mechanical properties of Mg–Li binary alloys limit their wide applications. Therefore, to obtain high-performance Mg–Li alloys, alloying elements, such as Mn, Zn, Al, Zr, and RE, are commonly used to improve performance. It has been reported that the addition of Mn alloying elements enhances their mechanical properties and corrosion resistance [4, 5].

Mg–Li–Mn alloys have become very attractive in recent years because of their low densities and excellent mechanical properties [4, 5]. Almost all of the Mg–Li–Mn alloys are conventionally prepared by directly mixing and fusing the three metallic elements. This conventional method has some drawbacks, such as a complicated process of production, problems of serious metal oxidation, and a high energy cost. Therefore, electrochemical methods for the preparation of magnesium base alloys are

K. Ye · M. L. Zhang (✉) · Y. Chen · W. Han · Y. De Yan · S. Q. Wei · L. J. Chen

Key Laboratory of Superlight Materials and Surface Technology, Ministry of Education, College of Materials Science and Chemical Engineering, Harbin Engineering University, Harbin 150001, People's Republic of China  
e-mail: zhangmilin2009@sina.com

drawing increased attention. In our previous study, we have successfully prepared Mg–Li alloys on a magnesium cathode from the LiCl–KCl melts and investigated the electrochemical formation process and phase control of Mg–Li alloys at 693–783 K [6, 7]. However, in these methods, remaining some shortcomings include a long process time and high energy consumption. These disadvantages originate from producing the corresponding metallic cathode materials and still cannot be eliminated.

Recently, our group proposed a new approach for the direct preparation of Mg–Li–Mn alloys via electrochemical codeposition of Mg, Li, and Mn from LiCl–KCl–MgCl<sub>2</sub>–MnCl<sub>2</sub> melts. The process is simpler than the former methods. Deposition and electrochemical studies of pure metallic magnesium and lithium have been an area of research. For example, Martínez and coworkers [8–11] have investigated the electrodeposition of magnesium ions in CaCl<sub>2</sub>–NaCl, CaCl<sub>2</sub>–NaCl–KCl, eutectic LiCl–KCl, and MgCl<sub>2</sub>–MgF<sub>2</sub> melts. Carlin and Osteryoung [12] reported on the deposition studies of lithium and bismuth at tungsten microelectrodes in LiCl–KCl eutectic. Piersma and Ryan [13] investigated the electrodeposition and stripping of lithium on inert electrodes in room-temperature chloroaluminate molten salts. However, the codeposition of Mg–Li–Mn ternary alloys has not been investigated even though the electrochemical codeposition method has been widely used to prepare alloys. For instance, Tsuda et al. [14–16] produced a series of Al-based alloys by codeposition from the molten salts of aluminum chloride-1-ethyl-3-methylimidazolium chloride. Ueda et al. [17] reported the codeposition of Al–Cr–Ni alloys using constant potential and potential pulse techniques in AlCl<sub>3</sub>–NaCl–KCl molten salt. Yan and coworkers [18–20] investigated the preparation of Mg–Li alloys by codeposition of Mg and Li on an inert electrode from LiCl–KCl–MgCl<sub>2</sub> melts, and studied the electrochemical study of the codeposition of Mg–Li–Zn alloys and Mg–Li–Al alloys from corresponding chloride melts. Tsuda et al. [21, 22] investigated the electrodeposition of Al–Mo–Mn and Al–Mo–Ti ternary alloys in AlCl<sub>3</sub>–EtMeImCl and related room-temperature molten salts.

In this study, we investigated the codeposition of Mg–Li–Mn alloys from LiCl–KCl–MgCl<sub>2</sub>–MnCl<sub>2</sub> melts by employing a series of electrochemical techniques. The Mg–Li–Mn alloys with different phases were prepared by galvanostatic electrolysis.

## 2 Experimental

### 2.1 Preparation and purification of the melts

The LiCl–KCl mixture (50:50 wt%, analytical grade) was contained in an alumina crucible placed in a quartz cell

located in an electric furnace. The temperature of melts was measured with a nickel–chromium thermocouple sheathed by an alumina tube. The mixture was dried under vacuum for more than 72 h at 573 K to remove excess water. Following this dehydration procedure, metal ion impurities were further removed by pre-electrolysis for 4 h at –1.8 V (vs. Ag/AgCl). Magnesium and manganese ions were introduced into the bath in the form of dehydrated MgCl<sub>2</sub> and MnCl<sub>2</sub> powder. All experiments were performed under an argon atmosphere.

### 2.2 Electrochemical apparatus and electrodes

The electrochemical techniques were performed using Im6eX electrochemical workstation (Zahner Co., Ltd.) with the THALES 3.08 software package. Ag/AgCl was used as reference electrode, which was constituted by a silver wire ( $d = 1$  mm) dipped into a quartz tube containing a solution of AgCl (1 wt%) in LiCl–KCl melts. All of the potentials were referred to the Ag/AgCl couple. The working electrode is molybdenum ( $d = 0.9$  mm, 99.99% purity). A spectral pure graphite rod ( $d = 8$  mm) served as the counter electrode. The lower end of the molybdenum working electrode was polished thoroughly using SiC paper, and then cleaned in ethanol using ultrasonic cleaning. The active electrode surface was determined after each experiment by measuring the immersion depth of the electrode in the molten salts.

### 2.3 Auxiliary techniques

The samples of Mg–Li–Mn alloys were prepared by galvanostatic electrolysis under different conditions. After the electrolysis, all samples were washed by hexane (99.8% purity), which hardly reacts with the Mg–Li alloys, to remove salts and stored in a glove box for analysis. These deposits were analyzed by XRD (Multi Flex TTR-III; Rigaku Industrial Corp. Ltd.) using Cu  $K_{\alpha}$  radiation at 40 kV and 150 mA. The specimens for OM (DFC320; Leica Microsystems) were mounted in thermosetting resins using a metallographic mounting press and then mechanically polished, and finally etched with a solution of 2 vol% HNO<sub>3</sub> in alcohol. The etching time was 30–60 s. The microstructure and micro-zone chemical analysis were also measured using SEM, EDS, and EPMA (JSM-6480A; JEOL Co., Ltd.). The samples for SEM/EDS/EPMA were polished and etched again using the former method and time. In order to determine Mg, Li, and Mn contents of the deposits, each deposit was dissolved in aqua regia (HNO<sub>3</sub>:HCl:H<sub>2</sub>O = 1:3:8, v/v). The solution was diluted and analyzed using an inductively coupled plasma atomic emission spectrometer (ICP-AES, Thermo Elemental, IRIS Intrepid II XSP).

### 3 Results and discussions

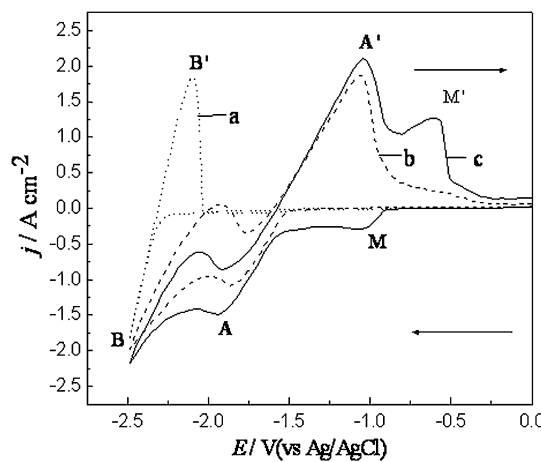
#### 3.1 Cyclic voltammetry

Figure 1 shows typical cyclic voltammograms obtained at molybdenum electrodes before and after the addition of 8 wt%  $MgCl_2$  and 2 wt%  $MnCl_2$  in  $LiCl-KCl$  melts at 893 K. The dotted curve (a) represents the voltammogram before the addition of  $MgCl_2$  and  $MnCl_2$ . Only one couple of cathodic/anodic (B/B') signals is observed which corresponds to the deposition and dissolution of liquid Li. The dash curve (b) shows the voltammogram measured after the addition of 8 wt%  $MgCl_2$ . Peaks A and B in the negative-going scan are ascribed to the formation of a three-dimensional (3D) phase [19, 20] of Mg and Li, respectively, because the deposition potential of Mg ions is more positive than that of Li ions in a chloride system [18]. Peaks B' and A' in the positive-going scan correspond to the dissolution of Li and Mg deposit, respectively. Before the addition of  $MgCl_2$ , reduction of Li(I) starts at about -2.24 V on a molybdenum electrode; after the addition of  $MgCl_2$ , reduction of Li(I) starts at approximately -2.01 V, respectively. In this way, the potential of Li metal deposition after the addition  $MgCl_2$  is more positive than the one of Li metal deposition before the addition. The potential shift is due to a lowering of activity of the deposited metal (Li) in other foreign substrate. The foreign substrate is probably Mg metal pre-deposited on the molybdenum electrode. The solid curve (c) exhibits the voltammogram measured after the addition of 8 wt%  $MgCl_2$  and 2 wt%  $MnCl_2$  over a potential range 0 to -2.5 V. In the negative potential region, steep increase in the cathodic (peak M) observed at about -0.90 V is

attributed to the deposition of Mn. In the positive potential region, peak M' is ascribed to dissolution of Mn. Similarly, peaks A/A' and B/B' originated from the deposition/dissolution of Mg and Li appeared, respectively. The reductions of ions of Mn, Mg, and Li start at approximately -0.90, -1.55, and -2.08 V, respectively. And the potential of Li metal deposition after the addition  $MgCl_2$  and  $MnCl_2$  is more positive than the one of Li metal deposition before the addition, too.

#### 3.2 Chronopotentiometry

Chronopotentiometric experiment was carried out to further study the formation of Mg–Li–Mn alloys. Figure 2 presents chronopotentiograms measured on a molybdenum electrode ( $S = 0.28 \text{ cm}^2$ ) in the  $LiCl-KCl-MgCl_2$  (8 wt%) melts containing 2 wt%  $MnCl_2$  at various applied current intensities at 893 K. The first plateau 1 should be associated to the reduction of Mn(II). At a cathodic current more negative than -75 mA (current density  $-0.27 \text{ A cm}^{-2}$ ), the curves exhibit two potential plateaus (plateaus 1 and 2), which are associated with the reduction of manganese and magnesium ions to the corresponding metals, respectively. At this current intensity, codeposition of Mn and Mg occurs. According to the phase diagram of Mg–Mn system [23], a second plateau 2 is due to the formation of Mg–Mn alloys. When the current reaches -400 mA ( $-1.43 \text{ A cm}^{-2}$ ), a third plateau 3 appears. This plateau is caused by a reduction of lithium ions. At this current intensity, codeposition of Mg, Li, and Mn occurs. It is obvious that the potential ranges for deposition of Mg, Li, and Mn are the same as those observed in the cyclic voltammograms in Sect. 3.1.



**Fig. 1** Cyclic voltammograms for the  $LiCl-KCl$  eutectic melts on a molybdenum electrode ( $S = 0.28 \text{ cm}^2$ ) at 893 K. (a) Containing 0 wt%  $MgCl_2$  and 0 wt%  $MnCl_2$ ; (b) containing 8 wt%  $MgCl_2$  and 0 wt%  $MnCl_2$ ; (c) containing 8 wt%  $MgCl_2$  and 2 wt%  $MnCl_2$ . Scan rate: 100 mV s<sup>-1</sup>

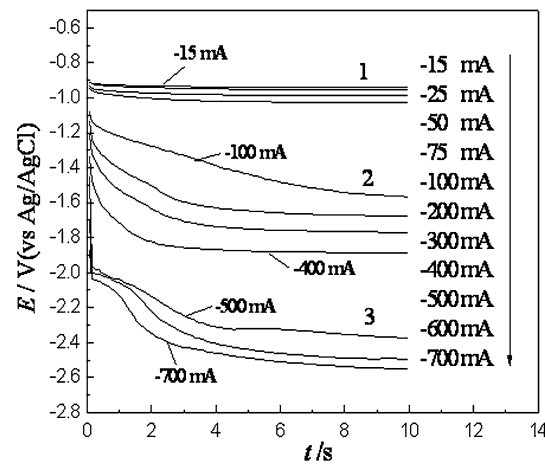


**Fig. 2** Chronopotentiograms obtained at various applied current intensities on a molybdenum electrode ( $S = 0.28 \text{ cm}^2$ ) in the  $LiCl-KCl-MgCl_2$  (8 wt%) melts containing 2 wt%  $MnCl_2$  at 893 K

### 3.3 Chronoamperometry

Chronoamperometry was employed to further investigate the electrochemical formation of Mg–Li–Mn alloys via codeposition of Mg, Li, and Mn. The chronoamperometric curves show typical features of a reduction process controlled by planar diffusion (as shown in Fig. 3). Clearly, the total current density at an applied potential of  $-1.000\text{ V}$  is significantly higher than those at a potential above  $-1.000\text{ V}$ , indicating that Mn(II) starts to be reduced. Moreover, the current density significantly increases when the step potential is changed from  $-1.500$  to  $-1.600\text{ V}$ , indicating that the reduction of Mn(II) is accompanied by that of Mg(II). The first formed alloy is that of Mg–Mn when the applied potential is more negative than  $-1.600\text{ V}$ . Figure 4 shows chronoamperometry with more

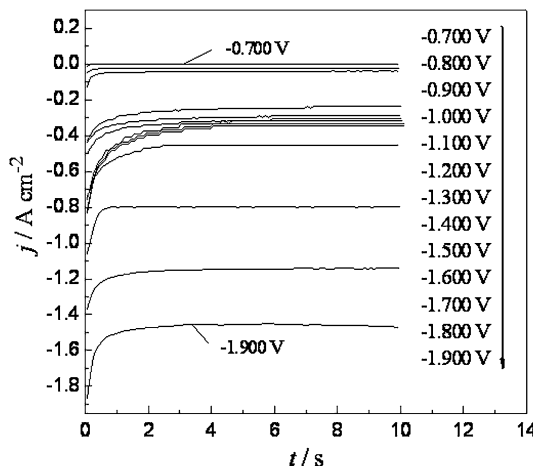


**Fig. 3** Chronoamperograms for the LiCl–KCl–MgCl<sub>2</sub> (8 wt%) melts containing 2 wt% MnCl<sub>2</sub> on a molybdenum electrode ( $S = 0.28\text{ cm}^2$ ) at various applied potentials at 893 K

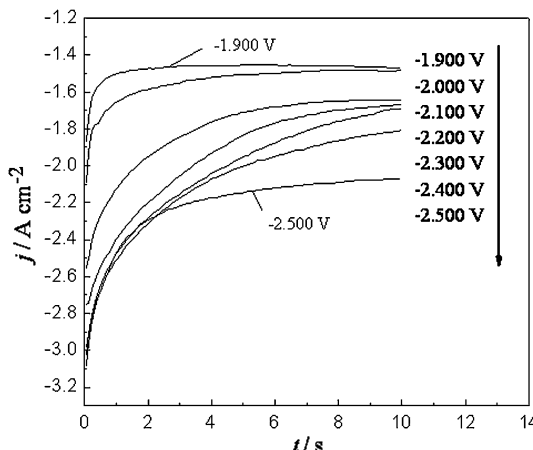


**Fig. 4** Chronoamperograms for the LiCl–KCl–MgCl<sub>2</sub> (8 wt%) melts containing 2 wt% MnCl<sub>2</sub> on a molybdenum electrode ( $S = 0.28\text{ cm}^2$ ) at more negative applied potentials at 893 K

negative applied potentials on a molybdenum electrode. When the step potential is changed from  $-2.000$  to  $-2.100\text{ V}$ , the current density increases rapidly again, which shows that Li(I) also starts to be reduced. Therefore, it can be concluded that at applied potentials more negative than  $-2.100\text{ V}$ , the codeposition of Mg, Li, and Mn occurs. In addition, the potential ranges of deposition of Mg, Li, and Mn are the same as those observed in the cyclic voltammograms and chronopotentiograms.

### 3.4 Galvanostatic electrolysis and characterization of the deposits

Based on the results obtained by CVs, chronopotentiometry and chronoamperometry, galvanostatic electrolysis was carried out in LiCl–KCl melts containing MgCl<sub>2</sub> and MnCl<sub>2</sub> with different concentrations on molybdenum electrodes at 893 K. Figure 5 shows the XRD patterns of Mg–Li–Mn alloy samples obtained by galvanostatic electrolysis from the LiCl–KCl melts containing 6–11 wt% MgCl<sub>2</sub> and 2 wt% MnCl<sub>2</sub> at  $7.14\text{ A cm}^{-2}$  for 2 h. The observed peaks were identified as  $\alpha$ -Mg,  $\beta$ -Li, and Mn phase (JCPDS No. 35-0821, No. 15-0401 and No. 65-1797). As seen from the XRD patterns, the Mg–Li–Mn alloys are composed of  $\alpha + \text{Mn}$ ,  $(\alpha + \beta) + \text{Mn}$ , and  $\beta + \text{Mn}$  phases. In patterns a–c, all Mg–Li–Mn alloys contain the Mn phase, which proves that intermetallic compound is not formed in Mg–Li–Mn alloys at this temperature. According to the phase diagram of the Mg–Mn and Li–Mn system [23], the concentration of Mn will be small in Mg–Li alloys since the solubility of Mn in Mg is around 0.8 at.% and Mn is insoluble in Li metal at

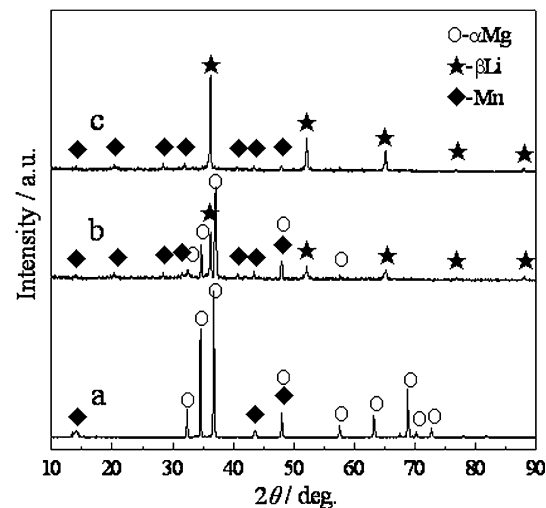
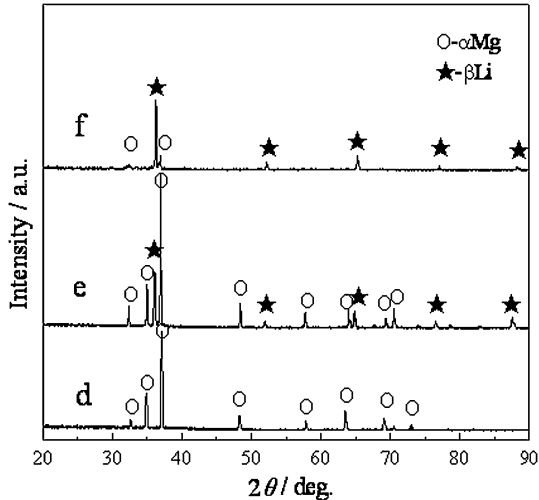


**Fig. 5** XRD patterns of deposits obtained by galvanostatic electrolysis on Mo electrodes ( $S = 0.28\text{ cm}^2$ ) in the LiCl–KCl melts with (a) 11 wt% MgCl<sub>2</sub> and 2 wt% MnCl<sub>2</sub>; (b) 8 wt% MgCl<sub>2</sub> and 2 wt% MnCl<sub>2</sub>; (c) 6 wt% MgCl<sub>2</sub> and 2 wt% MnCl<sub>2</sub> at  $2.00\text{ A}$  for 2 h at 893 K

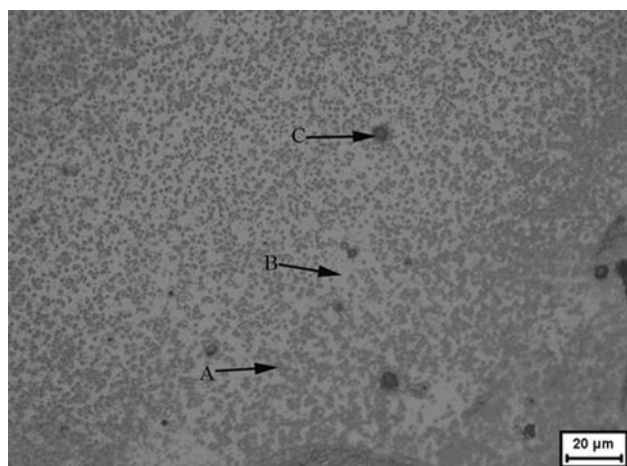
893 K. Moreover, the lithium contents of Mg–Li–Mn alloys increase (from  $\alpha$ ,  $\alpha + \beta$  to  $\beta$  phase) with the decrease of  $MgCl_2$  concentrations in the LiCl–KCl– $MnCl_2$  (2 wt%) melts at constant current intensity. Therefore, under the condition of electrolysis, the lithium contents and phase composition of Mg–Li–Mn alloys are adjustable simply by changing concentrations of  $MgCl_2$  and the electrolytic parameters.

Figure 6 shows the XRD patterns of typical  $\alpha$ ,  $\alpha + \beta$ , and  $\beta$  phases (correspond to patterns d, e, and f, respectively), Mg–Li–Mn alloys obtained by galvanostatic electrolysis from the LiCl–KCl– $MgCl_2$  melts containing relatively low concentration of  $MnCl_2$  (0.3 wt%) at  $7.14\text{ A cm}^{-2}$  for 2 h. Phase structure of the Mg–Li–Mn alloys obviously became simple (the Mn phase disappears) from the result of XRD, as the concentration of  $MnCl_2$  was decreased. It is obvious that the manganese content of Mg–Li–Mn alloy decreases with the decrease of the concentration of  $MnCl_2$  in LiCl–KCl– $MgCl_2$  melts. Mn has no apparent effect on the phase structure of Mg–Li alloys because of relatively low Mn contents in Mg–Li–Mn alloys. When the concentration of  $MgCl_2$  in the LiCl–KCl– $MnCl_2$  (0.3 wt%) melts was decreased at constant current density, the same phase transformation (from  $\alpha$ ,  $\alpha + \beta$  to  $\beta$  phase) was observed. Based on these results, it can be concluded that the variation of phases of Mg–Li–Mn alloys depends on the change of  $MgCl_2$  and  $MnCl_2$  concentrations.

The microstructure of the Mg–Li–Mn alloy by codeposition from LiCl–KCl melts containing 8 wt%  $MgCl_2$  and 2 wt%  $MnCl_2$  on a molybdenum electrode at 893 K exhibits a dual-phase microstructure, as given in Fig. 7.



**Fig. 6** XRD patterns of deposits obtained by galvanostatic electrolysis on Mo electrodes ( $S = 0.28\text{ cm}^2$ ) in the LiCl–KCl melts containing (d) 11 wt%  $MgCl_2$  and 0.3 wt%  $MnCl_2$ ; (e) 8 wt%  $MgCl_2$  and 0.3 wt%  $MnCl_2$ ; (f) 6 wt%  $MgCl_2$  and 0.3 wt%  $MnCl_2$  at 2.00 A for 2 h at 893 K



**Fig. 7** Optical micrograph of the Mg–Li–Mn alloy by codeposition from the LiCl–KCl eutectic melts containing 8 wt%  $MgCl_2$  and 2 wt%  $MnCl_2$  on a molybdenum electrode ( $S = 0.28\text{ cm}^2$ ) at 2.00 A for 2 h at 893 K

The result of optical micrograph is in good agreement with the one obtained in the analysis of XRD. The dual-phase microstructure includes a  $\beta$  matrix plus a distributed  $\alpha$  phase. The dark A, bright B, and point C zones of the microstructure correspond to the  $\alpha$  phase,  $\beta$  phase, and Mn phase, respectively.

In order to estimate the main location of the distribution of the element Mn, an SEM equipped with EDS quantitative analysis was applied to further investigate the distribution of the element Mn. Figure 8 shows the SEM and EDS quantitative analysis of the Mg–Li–Mn alloy by codeposition from the LiCl–KCl eutectic melts containing 8 wt%  $MgCl_2$  and 2 wt%  $MnCl_2$ . The gray zone A in the SEM corresponds to the dark  $\alpha$  phase in the optical micrograph; the black zone B in the SEM corresponds to the bright  $\beta$  matrix in the optical micrograph. Moreover, according to the phase diagram of the Mg–Mn and Li–Mn system [23], the concentration of Mn will be small in Mg–Li alloys since the solubility of Mn in Mg is around 0.8 at.% and Mn is insoluble in Li metal at 893 K. Thus, the observed white spots C in the SEM correspond to the black spots in the optical micrograph, which is associated to the deposition of Mn metal. The EDS result of the zone of labeled 001 taken from  $\alpha$  phase,  $\beta$  matrix, and white spots indicates that the deposits are composed of the elements of Mg and Mn. As windows in front of the Si(Li) detector can absorb low-energy X-rays, EDS detectors cannot detect presence of elements with atomic number less than 4, meaning that EDS cannot detect element Li. At the same time, a mapping analysis of the elements was employed to further examine the uniformity of elements of Mg and Mn distributed in the Mg–Li–Mn alloy. Figure 9 shows a EDS mapping analysis of the Mg–Li–Mn alloy by

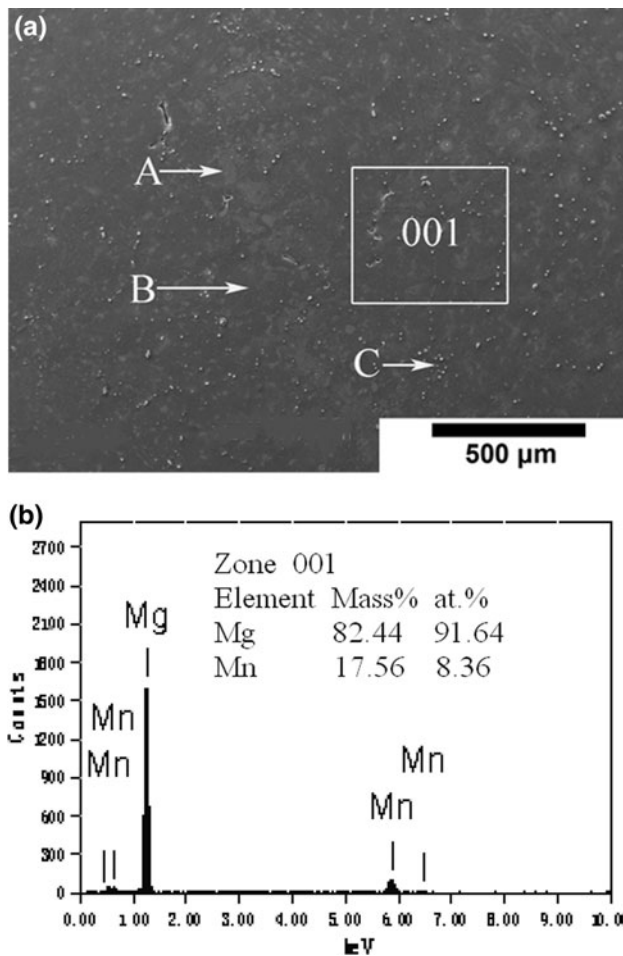


**Fig. 8** SEM and EDS analysis (weight percentage (Mass%); atom percentage (at. %)) of the Mg–Li–Mn alloy by codeposition from the LiCl–KCl–MgCl<sub>2</sub> (8 wt%) melts containing 2 wt% MnCl<sub>2</sub> on a molybdenum electrode ( $S = 0.28 \text{ cm}^2$ ) at 2.00 A for 2 h at 893 K

codeposition from LiCl–KCl eutectic melts containing 8 wt% MgCl<sub>2</sub> and 2 wt% MnCl<sub>2</sub>. From the SEM and EPMA analysis, it was confirmed that the elements of Mg and Mn were formed on the whole surface and distributed homogeneously in the obtained Mg–Li–Mn alloy deposits.

EDS is a qualitative and semiquantitative estimate of elemental concentration, and element Li cannot be detected in the EDS. Therefore, the ICP analysis of alloys was carried out. The ICP analyses of all samples obtained by galvanostatic electrolysis are listed in Table 1. The composition analysis results from EDS (Fig. 8) distinguished from that of ICP (Table 1). Considering the fact that Li presented in ICP analysis was not detected in the EDS and error of EDS measurement, the differences of ICP and EDS should be reasonable. The ICP results show that the chemical compositions of Mg–Li–Mn alloys are consistent with the phase structures of the XRD patterns, and the Mg–Li–Mn alloy (codeposition from LiCl–KCl 8 wt% to MgCl<sub>2</sub> 2 wt% MnCl<sub>2</sub> melts) used for the analysis of SEM

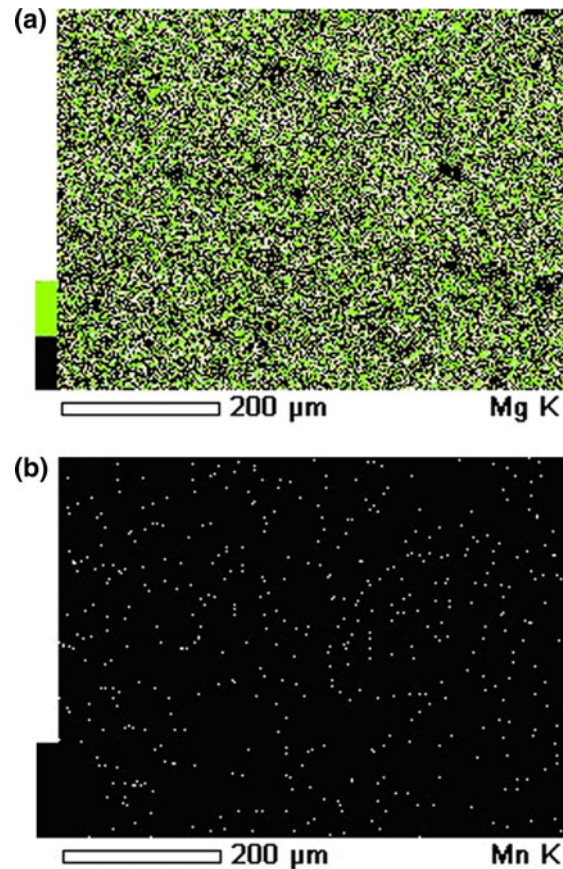


**Fig. 9** EDS mapping analysis of the Mg–Li–Mn alloy by codeposition from the LiCl–KCl–MgCl<sub>2</sub> (8 wt%) melts containing 2 wt% MnCl<sub>2</sub> on a molybdenum electrode ( $S = 0.28 \text{ cm}^2$ ) at 2.00 A for 2 h at 893 K. **a** Area analysis by Mg  $K_\alpha$  and **b** area analysis by Mn  $K_\alpha$

and EDS is identified as Mg–9.1 Li–2.5 Mn alloy. Under galvanostatic electrolysis, the lower MgCl<sub>2</sub> concentration in the LiCl–KCl melts with equivalent MnCl<sub>2</sub> concentration at a constant current intensity, the higher the lithium content of Mg–Li–Mn alloys. Under the same MgCl<sub>2</sub> concentration (8 wt%) in the LiCl–KCl–MgCl<sub>2</sub> melts, the manganese contents of Mg–Li–Mn alloys increase with the increasing MnCl<sub>2</sub> concentrations.  $\alpha$ ,  $\alpha + \beta$ , and  $\beta$  phases Mg–Li–Mn alloys with different manganese contents (0.08–3.10 wt%) were obtained by galvanostatic electrolysis at 7.14 A cm<sup>-2</sup> for 2 h. When the manganese content of magnesium alloys is close to 1.5 wt%, the corrosion rate of corresponding magnesium alloys is reduced to the minimum in seawater. Consequently, the manganese contents of Mg–Li–Mn alloys are generally controlled between 1.3 and 2.5 wt% [24]. Therefore, one way to obtain optimal corrosion resistance and mechanical properties is to reduce the Mn content under its solid solubility limitation (solid solubility limitation of Mn in Mg–Li alloy is 5.9 wt%). Under the condition of electrolysis, an approach of decreasing Mn content in Mg–Li–Mn alloy is to reduce the

**Table 1** The ICP analyses of all samples obtained by galvanostatic electrolysis ( $7.14 \text{ A cm}^{-2}$ ) on Mo electrodes ( $S = 0.28 \text{ cm}^2$ ) from the LiCl–KCl melts containing different  $\text{MgCl}_2$  and  $\text{MnCl}_2$  concentrations for 2 h at 893 K

Samples	$\text{MgCl}_2$ concentration (wt%)	$\text{MnCl}_2$ concentration (wt%)	Li content (wt%)	Mn content (wt%)	Mg content (wt%)
1	6	2	40.62	2.08	Bal.
2	8	2	9.07	2.45	Bal.
3	11	2	2.12	2.63	Bal.
4	8	1	10.12	0.97	Bal.
5	8	3	5.98	2.88	Bal.
6	8	4	3.43	3.10	Bal.
7	6	0.3	43.37	0.08	Bal.
8	8	0.3	10.04	0.19	Bal.
9	11	0.3	2.45	0.31	Bal.

concentration of  $\text{MnCl}_2$  in the LiCl–KCl– $\text{MgCl}_2$ – $\text{MnCl}_2$  melts. Based on these results, it can be concluded that the lithium and manganese contents of Mg–Li–Mn alloys can be adjusted by changing the  $\text{MgCl}_2$  and  $\text{MnCl}_2$  concentrations.

#### 4 Conclusions

The electrochemical codeposition behavior of Mg, Li, and Mn on Mo electrodes in LiCl–KCl (50:50 wt%) melts containing different concentrations of  $\text{MgCl}_2$  and  $\text{MnCl}_2$  was investigated at 893 K. According to studies of codeposition conditions, Mg–Li–Mn alloys can be directly prepared via codeposition of Mg, Li, and Mn on inert electrodes from LiCl–KCl– $\text{MgCl}_2$ – $\text{MnCl}_2$  melts. Typical  $\alpha$ ,  $\alpha + \beta$ , and  $\beta$  phases Mg–Li–Mn alloys with different lithium and manganese contents were obtained by galvanostatic electrolysis on molybdenum electrodes at cathodic current density  $7.14 \text{ A cm}^{-2}$  for 2 h at 893 K. The lithium and manganese contents of Mg–Li–Mn alloys can be controlled by  $\text{MgCl}_2$  and  $\text{MnCl}_2$  concentrations. Direct preparation of Mg–Li–Mn alloys by electrolysis using  $\text{MgCl}_2$ , LiCl, and  $\text{MnCl}_2$  as raw materials could revolutionize industrial production of Mg–Li–Mn alloys.

**Acknowledgments** This study was financially supported by the 863 project of the Ministry of Science and Technology of China (2006AA03Z510), the National Natural Science Foundation of China (50871033), the Scientific Technology Project of Heilongjiang Province (GC06A212), and the Scientific Technology Bureau of Harbin (2006PFXXG006).

#### References

- Wang S, Wu G, Li R et al (2006) Mater Lett 60:1863
- Drozd Z, Trojanová Z, Kúdela S (2004) J Alloys Compd 378:192
- Sanschagrin A, Tremblay R, Angers R et al (1996) Mater Sci Eng A 220:69
- Li H, Ji H, Yao G et al (2006) Chin J Process Eng 6:491 (in Chinese)
- Li H (2009) Mater Heat Treat 38:12 (in Chinese)
- Yan Y, Zhang M, Han W et al (2008) Electrochim Acta 53:3323
- Zhang M, Yan Y, Hou Z et al (2007) J Alloys Compd 440:362
- Castrillejo Y, Martínez AM, Pardo R et al (1997) Electrochim Acta 42:1869
- Martínez AM, Børresen B, Haarberg GM et al (2004) J Electrochem Soc 151:C508
- Martínez AM, Børresen B, Haarberg GM et al (2004) J Appl Electrochem 34:1271
- Børresen B, Haarberg GM, Tunold R (1997) Electrochim Acta 42:1613
- Carlin RT, Osteryoung RA (1989) J Electrochem Soc 136:1249
- Piersma BJ, Ryan DM (1996) J Electrochem Soc 143:908
- Tsuda T, Hussey CL, Stafford GR et al (2003) J Electrochem Soc 150:C234
- Tsuda T, Hussey CL, Stafford GR (2004) J Electrochem Soc 151:C379
- Tsuda T, Hussey CL, Stafford GR et al (2004) J Electrochem Soc 151:C447
- Ueda M, Kigawa H, Ohtsuka T (2007) Electrochim Acta 52:2515
- Yan Y, Zhang M, Han W et al (2008) Chem Lett 37:212
- Yan Y, Zhang M, Xue Y et al (2009) Electrochim Acta 54:3387
- Yan Y, Zhang M, Xue Y et al (2009) J Appl Electrochem 39:455
- Tsuda T, Hussey CL, Stafford GR (2005) J Electrochim Soc 152:C620
- Tsuda T, Arimoto S, Kuwabata S et al (2008) J Electrochim Soc 155:D256
- Massalski TB, Murray JL, Benett LH et al (1990) Binary alloy phase diagrams. American Society for Metals, Metals Park
- Wang D, Zhang J, Du H et al (2005) Res Stud Foundry Equip 1:12 (in Chinese)